INTEGRATED CO$_2$ CORROSION - MULTIPHASE FLOW MODEL

Srdjan Nesic, Shihuai Wang, Jiyong Cai and Ying Xiao
Institute for Corrosion and Multiphase Technology
Ohio University, Athens, OH 45701

ABSTRACT

An integrated CO$_2$ corrosion – multiphase flow model was built which takes into account the effect of most important variables. The model is mechanistic in nature and resides on clear theoretical foundations. All the assumptions in the model are explicitly stated and are open to future adjustments and improvements.

The overall model was extensively verified with a large experimental database and was able to perform reasonably well in all cases. The multiphase flow model was also benchmarked against a well-established commercial package.

Keywords: model, CO$_2$ corrosion, multiphase flow, software

INTRODUCTION

A variety of prediction models for CO$_2$ corrosion of carbon steel exist.[1-19] Most of these models are semi-empirical, or even fully empirical with only a handful of the more recent models being based on mechanistic descriptions of the processes underlying CO$_2$ corrosion[14-19]. A recent paper by Nyborg[20] reviews the performance of a representative group of models concluding that most of the models predict well the "worst case" CO$_2$ corrosion rate but vary widely when more complex effects (e.g. protective films, water entrainment/wetting, H$_2$S, etc) are included. The main reason for this spread lies in the arbitrary nature of the empirical correction factors that are employed to account for the various complicating effects.

The present paper describes a newly developed CO_2 corrosion multiphase flow model that takes into account the effect of most important variables. The majority of the model is mechanistic in nature, fully transparent and resides on solid theoretical foundations. Some aspects of the model that cover areas where insufficient knowledge exists (e.g. H_2S effect) employ a semi-empirical approach. It should be noted that the current model is a decade long project building on previous developments published in the open literature[21-23].

INTEGRATED MODEL

The integrated model consists of two main models: the *corrosion model* and the *multiphase flow model*. An interface module enables the transfer of the data between the two.

Corrosion model

The transient mechanistic CO_2 corrosion model of Nesic et al. [21-23] is used as the backbone of the corrosion model of the integrated package. The corrosion model comprises of the following sub-models covering:
- Kinetics of electrochemical reactions at the steel surface including:
    - H^+ reduction
    - H_2CO_3 reduction
    - HAc reduction
    - Fe oxidation
- Transient one-dimensional transport of species between the bulk solution and the steel surface, through the turbulent boundary layer and through a porous surface film.
- Kinetics of chemical reactions including precipitation.
- Growth of iron carbonate films.
- Effect of traces of H_2S.
- Effect of steel type.
- Effect of inhibition by crude oil and/or corrosion inhibitors.
- Possibility and morphology of localized attack.

The physical, mathematical and numerical aspects of the electrochemical, transport and chemical models have been published previously, and only a very brief outline is given below to facilitate the understanding of the text to follow.

Electrochemical Reactions at the Steel Surface

As the CO_2 corrosion process is electrochemical in nature, the corrosion rate can be explicitly determined by calculating the rate of the electrochemical reactions underlying it such as: iron oxidation as well as reductions of hydrogen ion, carbonic and acetic acid. The electrochemical reaction rate can be expressed as a current density, i

(expressed in $A\ m^{-2}$), which is a function of the potential at the metal surface, E (expressed in V):

$$i = \pm\, i_o \cdot 10^{\pm\frac{E-E_{rev}}{b}} \cdot \prod_{s=1}^{n_s}\left(1-\theta_s\right) \tag{1}$$

This equation is unique for each of the electrochemical reactions involved in a corrosion process such as hydrogen reduction, iron oxidation, etc. The "+" sign applies for anodic reactions while the "–" sign applies for cathodic reactions. θ_s is the fraction of the steel surface where a given electrochemical reaction does not occur because the surface is covered by a species s which could be an adsorbed inhibitor or a protective film. The product sign $\prod$ accounts for a compounding (additive) effect by more than one surface species. For each electrochemical reaction, equation (1) is different because of the parameters defining it: i_o - the exchange current density in $A\ m^{-2}$, E_{rev} - the reversible potential in V, and b - the Tafel slope in V. These parameters have to be determined experimentally and are functions of temperature and in some cases species concentrations. An overview covering how these parameters are calculated in the present model is given elsewhere (reference [24] for the cathodic reaction and reference [25] for the anodic reaction). The unknown electrical potential at the metal surface E in (1), is also called corrosion potential or open circuit potential, which can be found from the current balance equation at the metal surface:

$$\sum_{a=1}^{n_a} i_a = \sum_{c=1}^{n_c} i_c \tag{2}$$

where n_a and n_c are the total number of anodic and cathodic reactions respectively.

Transport Processes in the Surface Film and in the Boundary Layer

In corrosion, certain species in the solution are "produced" at the steel surface (e.g. Fe^{2+}) while others are depleted (e.g. H^+). This leads to concentration gradients and diffusion of these species towards and away from the surface. On the other hand the rate of the electrochemical reactions depends on the species concentrations at the steel surface. Therefore, there exists a two-way coupling between the electrochemical processes at the metal surface (corrosion) and transport processes in the adjacent solution layer (i.e. diffusion in the boundary layer). Flow i.e. turbulent eddies can penetrate deep into the boundary layer and significantly enhance the rate of species transport to and from the surface, hence leading to a higher corrosion rate. Conversely, when protective films form on the steel surface, they may slow down the diffusion of species and can reduce the corrosion rate.

In a model of uniform corrosion, a one-dimensional species transport domain is sufficient, stretching from the steel surface through the pores of a surface film and the mass transfer boundary layer, ending in the turbulent bulk of the solution, as sketched in FIGURE 1. The concentration of each species is governed by a species conservation

(mass balance) equation. A universal form of the equation which describes transport for species j in the presence of chemical reactions (discussed below), which is valid both for the liquid boundary layer and the porous film, is:

$$\underbrace{\frac{\partial(\varepsilon c_j)}{\partial t}}_{\text{accumulation}} = \underbrace{\frac{\partial}{\partial x}\left(\varepsilon^{1.5} D_j^{\text{eff}} \frac{\partial c_j}{\partial x}\right)}_{\text{net flux}} + \underbrace{\varepsilon R_j}_{\substack{\text{source or sink} \\ \text{due to chemical reactions}}} \tag{3}$$

where c_j is the concentration of species j in $kmol\ m^{-3}$, ε is the porosity of the film, $D_j^{\text{eff}} = D_j^m + D_j^t$ is the effective diffusion coefficient of species j, in $m^2\ s^{-1}$, which includes both the molecular component, D_j^m, and the turbulent component, D_j^t. Turbulent convection has been modeled by *turbulent diffusion* as the former is difficult to determine explicitly. The source or sink R_j of species j is due to all the chemical reactions in which the particular species is involved in $kmol\ m^{-3}s^{-1}$. t is time in s and x is the spatial coordinate in m. It should be noted that in the transport equation above electromigration has been neglected as its contribution to the overall flux of species is small.

One equation of the form (3) is written for each species in the solution. The resulting set of equations is solved simultaneously in space and time. The boundary conditions for this set of partial differential equations are: (a) flux of species at the steel surface determined from the rate of the electrochemical reactions as given by equation (1) and (b) equilibrium concentrations of species in the bulk. The equilibrium is used also as the initial condition. Once the set of equations is solved for any given time step, the corrosion rate, CR, can be simply calculated as the flux of Fe^{2+} ions at the metal surface.

Chemical Reactions

A variety of chemical reactions may accompany the corrosion process, some homogeneous (occurring everywhere in the solution) others heterogeneous (occurring only at the metal surface). Hydration and dissociation are two typical homogenous chemical reactions accounted for in CO_2 corrosion. Precipitation of iron carbonate is the only heterogeneous chemical reaction considered in the present model. A list of all the chemical reactions included in the model is given elsewhere[21]. Most chemical reactions are very fast when compared to diffusion and electrochemical reactions (all occurring simultaneously in corrosion) and can maintain chemical equilibrium throughout the solution. Conversely, when some chemical reactions proceed slowly, other faster processes (such as electrochemical reactions or diffusion) can lead to local non-equilibrium in the solution. Either way, by affecting the surface concentrations of species, chemical reactions can significantly alter the rate of electrochemical processes at the steel surface and the rate of corrosion. This is particularly true when, due to high local concentrations of species solubility limit is exceeded and precipitation of surface films occurs.

Homogeneous chemical reactions. The rate of a homogeneous chemical reaction can be calculated, assuming ideal solutions and first order kinetics, as:

$$R_j = k_f \prod_{r=1}^{n_r} c_r - k_b \prod_{p=1}^{n_p} c_p \tag{4}$$

where k_f and k_b are the forward and backward reaction rate constants for the particular chemical reaction while c_r and c_p are the concentrations of reactants and products respectively. Generally, for any set of k chemical reactions involving j species one can write compactly:

$$R_j = a_{jk} r_k \tag{5}$$

where tensor notation applies for the subscripts, a_{jk} is the stoichiometric matrix where row j represents the j-th species, column k represents the k-th chemical reaction, and r_k is the reaction rate vector. More details about this approach is given elsewhere.[21] Using this technique any number of homogenous chemical reactions can be added to the model with little effort.

Heterogeneous chemical reactions. The rate of precipitation of iron carbonate $R_{FeCO_{3(s)}}$ can be described as a function of supersaturation S, the solubility limit K_{sp}, temperature T and surface area-to-volume ratio A/V:

$$R_{FeCO_{3(s)}} = \frac{A}{V} \cdot f(T) \cdot K_{sp} \cdot f(S) \tag{6}$$

Supersaturation is defined as:

$$S = \frac{c_{Fe^{2+}} c_{CO_3^{2-}}}{K_{sp}} \tag{7}$$

From the two different expressions describing the kinetics of iron carbonate precipitation proposed by Johnson and Tomson[26] and Van Hunnik et al.[27], the latter is used because it is believed to give more realistic results especially at higher supersaturation.

Growth of iron carbonate films

When iron carbonate precipitates at the steel surface, it can slow down the corrosion process by:

- presenting a diffusion barrier for the species involved in the corrosion process, i.e. by reducing the flux of species, accounted for by porosity ε in equation (3);

- blocking (covering) a portion of the steel surface and preventing the electrochemical reactions from happening there, as accounted for by surface coverage θ_s in equation (1) .

Iron carbonate film growth depends primarily on the precipitation rate, R_{FeCO_3} . As more iron carbonate precipitates the film can grow in density as well as thickness. However, the steel surface corrodes under the film, continuously creating a "void" between the film and the steel surface (here called "film undermining"). As soon as it is created, the void starts filling up by the ongoing precipitation. When the rate of precipitation at the steel surface equals or exceeds the rate of corrosion (film undermining) dense protective films form - sometimes very thin but still protective. Vice versa, when the corrosion process undermines the newly formed film faster than precipitation can fill in the voids, a porous and unprotective film forms - which can be sometimes very thick and still unprotective.

In the context of the present model, a mass balance equation for solid iron carbonate which includes the effect of undermining can be written and expressed in terms of volumetric film porosity ε :

$$\underbrace{\frac{\partial \varepsilon}{\partial t}}_{\substack{\text{film porosity} \\ \text{change}}} = \underbrace{-\frac{M_{FeCO_{3(s)}}}{\rho_{FeCO_{3(s)}}} R_{FeCO_{3(s)}}}_{\text{precipitation}} - \underbrace{CR \frac{\partial \varepsilon}{\partial x}}_{\text{undermining}} \tag{8}$$

Solution of this equation simultaneously with the transport equation (3) for various species and electrochemical equation (1) enables direct prediction of iron carbonate film thickness and porosity as well as its protective properties. More details about the film growth model are given elsewhere[21-23].

H₂S traces

Modeling of the effect of H₂S on CO₂ corrosion is still in its early stages, as not enough is known about the complex interactions that take place. Dissolved H₂S is certainly a mild acid and, if present in high enough concentrations, has to be treated as another cathodic species, in a similar way as carbonic and acetic acids. The presence of H₂S can lead to formation of various forms of iron sulfide films that can be very protective. In other cases they can lead to localized attack. Finally, elemental sulfur is often seen in conjunction with high H₂S concentrations, further complicating the situation.

At this point in time, for the purposes of modeling, there seems to be enough evidence about the effect of very small H₂S concentrations (traces of H₂S) on CO₂ corrosion at low pH, where precipitation of iron sulfides does not occur. For concentrations of H₂S below 500 ppm in the gas phase and for pH<5, a large number of carefully controlled corrosion experiments has been conducted in our laboratory over the past few years, at various temperatures (20-80°C), partial pressures of CO₂ (1-7 bar) and velocities (stagnant to 3 m/s) in both single and multiphase flow. All the data strongly suggest that the presence of even very small amounts of H₂S (10 ppm in the gas phase)

leads to rapid and significant reduction in the CO_2 corrosion rate. At higher H_2S concentrations this trend is arrested or even somewhat reversed (see FIGURE 2). The effect seems to be universal and depend solely on the H_2S concentration, as all the data obtained at very different conditions follow the same trend, as shown in FIGURE 2. The corrosion rate in FIGURE 2 was normalized with the "blank" corrosion rate, i.e. a CO_2 corrosion rate obtained without any H_2S present.

The investigation into the causes of this behavior is ongoing. The concentrations of H_2S involved in the abovementioned experiments were too low (ppm range) to consider H_2S as a significant cathodic species in the same way as carbonic or acetic acid. All the existing evidence points towards sulfide species, seen on the metal surface, as being responsible for the rapid decrease as well as the subsequent mild increase of the corrosion rate. It is hypothesized that sulfides play a double role: they inhibit the corrosion process by surface coverage (dominant at very low H_2S concentrations) and have a catalytic effect, e.g. by providing an increased area for the cathodic reaction (seen at higher H_2S concentrations). Therefore an equation including a simple Langmuir type adsorption isotherm and a first order catalytic effect was successfully used to model the decrease of the corrosion rate as seen in FIGURE 2:

$$1 - \theta_{H_2S} = \frac{1}{1 + K_{a/d}\, c_{H_2S}} + k_c\, c_{H_2S} \tag{9}$$

Here $K_{a/d}$ is the adsorption/desorption constant for sulfide species and k_c is the catalytic rate constant.

Steel type

The effect of steel type on corrosion rate has been modeled based on their electrochemical behavior in CO_2 solutions. The focus so far was primarily on low carbon (mild) steels and low-alloy steels typically used for pipelines. Four steels were included in the current model with others being investigated:

- Ferritic-perlitic
- Ferritic-perlitic with 1% Cr
- Tempered martensitic
- Tempered martensitic with 3% Ni

Polarization experiments have indicated that on the surface of these four steels, the cathodic reactions proceeded similarly. However, differences were seen in the corrosion rate, and they were ascribed to the different anodic dissolution rates stemming from different steel compositions and microstructures. This effect was modeled by using the experimental data to extract the electrochemical parameters specific for each steel needed to characterize its anodic behavior. As all the four steels listed above actively dissolved in CO_2 solutions, exchange current density, reversible potential and Tafel slope were determined for each steel. For passivating steels, one also needs to identify the passivation potential and current density and any pitting potential.

<u>Inhibition</u>

Two sources of corrosion inhibition were considered in the model: a) inhibition by addition of corrosion inhibitors and b) inhibition by components present in the crude oil.

Corrosion inhibitors. Modeling of the effect of corrosion inhibitors is not a straightforward task. There is a plethora of approaches in the open literature, varying from the use of simple *inhibitor factors* and *inhibition efficiencies* to the application of complicated *molecular modeling* techniques to describe inhibitor interactions with the steel surface and iron carbonate film. A middle-of-the-road approach has been used here which is based on the assumption that corrosion protection is achieved by *surface coverage*, i.e. that the inhibitor adsorbs onto the steel surface and prevents the electrochemical reactions from occurring on the underlying steel. The degree of protection is assumed to be directly proportional to the fraction of the steel surface covered by the inhibitor, as described by equation (1). In this model one needs to establish a relationship between the surface coverage θ and the inhibitor concentration in the solution c_{inh}. This is most commonly done by the use of adsorption isotherms. It has been shown[28] that the Frumkin isotherm can be successfully used to model the degree of protection offered by the inhibitor:

$$K_{a/d} c_{inh} = \left(\frac{\theta}{1-\theta} \right) e^{-f\theta} \qquad (10)$$

Experimental data from inhibitor testing have been used to identify the $K_{a/d}$ and f for a number of inhibitor formulations. When there is evidence that a particular inhibitor has differing effects on the cathodic and anodic reactions, unique constants can be identified from experiments and used for each individual reaction as described by equation (1).

Corrosion inhibition by crude oil. It has been known for a while that CO_2 corrosion rates seen in the field in the presence of crude oil are much lower than those obtained in laboratory conditions where crude oil was not used or so called "dead" or synthetic crude oil was used. One can identify two main effect of crude oil on the CO_2 corrosion rate.

The first is a *wettability* effect and relates to a hydrodynamic condition where crude oil entrains the water and prevents it from wetting the steel surface (continuously or intermittently). This effect has been included in the present model and will be discussed in more detail in the following section on multiphase flow.

The second effect is *corrosion inhibition* by certain components of the crude oil that reach the steel surface either by direct contact or by first partitioning into the water phase. Little is known about the nature and the effectiveness of these components which inhibit corrosion. A recent detailed study[29 -31] of the subject was used as a basis for the present model. There the degree of inhibition was quantitatively related to the chemical composition of the crude oil and in the first place to the concentration of saturates, aromatics, resins, asphaltenes, nitrogen and sulfur. In the present model, given a crude oil composition, the surface coverage by a crude oil inhibitor can be determined, leading to a reduction in corrosion rate as described by equation (1).

Localized Attack

The possibility of localized attack was modeled by using the modified two-dimensional stochastic algorithm first proposed by Pots[27]et al. The details of this development are described in a separate publication[32]. The algorithm uses a single input parameter, the scaling tendency:

$$ST = \frac{R_{FeCO_3(s)}}{CR} \qquad (11)$$

which is calculated by the mechanistic model presented above. When the mechanistic model predicts $ST=0$ (meanings that there is no precipitation), the algorithm predicts uniformly distributed corrosion attack as shown in FIGURE 3a. For high ST (high precipitation rates) the algorithm predicts a uniformly protected surface (FIGURE 3b). When ST is set somewhere in between, the algorithm predicts a partially protective film leading to localized corrosion attack (FIGURE 3c). It should be noted that the prediction is stochastic, i.e. given the same ST value, the algorithm leads to somewhat different surface morphologies every time the simulation is repeated.

Multiphase Flow Model

Pipelines frequently transport natural gas, water and crude oil simultaneously. Different flow patterns can be found most often being: stratified, slug or annular flow. In the liquid phase, water and oil can flow separated or mixed with either phase being continuous with the other flowing as a dispersed phase. Different flow patterns lead to a variety of steel surface wetting mechanisms which greatly affect corrosion.

To properly predict the corrosion rate in the pipelines, it is essential to understand the flow pattern and the associated flow properties as well as to know which liquid is in contact with the pipe wall. In this integrated corrosion/flow prediction package model, four main models are included in the multiphase flow model: flow pattern determination; water entrainment/wetting prediction and flow properties calculation. In the following sections, these three models will be briefly described.

Flow Pattern Determination

The procedure of flow pattern determination includes calculation of two main flow pattern transition criteria: *stratified to non-stratified* and *slug to annular flow* transitions. This enables building of a flow regime map and identification of a particular flow regime, given a set of input conditions.

Stratified to non-stratified flow transition. A well established model, which predicts the transition between gas-liquid stratified flow and non-stratified flow, stems from the model first proposed by Taitel and Dukler[33]. To simplify the prediction, oil and water are

treated as a single liquid phase. In this case, the momentum balance equations for the gas and liquid phases can be rewritten as:

$$-A_G\left(\frac{dP}{dx}\right) - \tau_{WG}S_G - \tau_i S_i - \rho_G A_G g \sin\theta = 0 \tag{12}$$

$$-A_L\left(\frac{dP}{dx}\right) - \tau_{WL}S_L + \tau_i S_i - \rho_L A_L g \sin\theta = 0 \tag{13}$$

where the subscripts G and L denote the gas phase and liquid phase respectively. τ is the shear stress and the subscripts WL, WG and i denote the various interfaces: liquid/wall, wall/gas and gas/liquid, respectively. S represents the pipe perimeter wetted by each phase. dP/dX denotes the pressure gradient. A_G and A_L are the cross sectional areas occupied by the gas phase and oil-water mixture. θ denotes the pipe inclination.

The shear stresses in equations (12) and (13) are given by the following relationships:

$$\tau_{WG} = \frac{f_G \rho_G U_G^2}{2} \qquad \tau_{WL} = \frac{f_L \rho_L U_L^2}{2} \qquad \tau_i = \frac{f_i \rho_G U_i^2}{2} \tag{14}$$

where f_G, f_L and f_i denote the friction factor for gas/wall, liquid/wall and gas/liquid interfaces, respectively. ρ denotes the density. U_G, U_L and U_i represent the in-situ velocity of gas, oil-water mixture and gas/liquid interface. In the present model f_G, f_L and f_i differ from those proposed by Taitel and Dukler[33]. The friction factor f_G is calculated with the equation proposed by Zagarola[34]. The liquid/wall fiction factor and the gas/liquid interfacial friction factor, f_L and f_i are determined by the correlations proposed by Petalas et al.[35] Once the liquid height is obtained by solving the momentum equations (12) and (13), an approach used by Taitel and Dukler[33], which uses an extension of the interfacial wave growth theory, is used to build the transition criteria from stratified to non-stratified flow.

Slug to annular flow transition. To obtain the slug to annular transition criterion the momentum equations, similar to (12) and (13), are solved accounting for the maximum slug void fraction (Jepson and Taylor)[36]. When the void fraction of the slug exceeds a critical value, the slug "blow through" occurs and the liquid is spread around the pipe circumference leading to annular flow.

Water Entrainment/Wetting Prediction

In the three main flow regimes discussed above (stratified, slug and annular) the liquid layer is in touch with the pipe wall. The key question is: which phase is continuous and if it is the oil phase, whether all water is entrained. A new unified approach, following Brauner[37] and Barnea[38], for predicting water-in-oil fully dispersed

flow will be discussed below. A criterion for forming stable water-in-oil dispersed flow was derived as the means of calculating the critical velocity for water entrainment within the liquid layer. Two main physical properties, *maximum droplet size* related to breakup and coalescence and *critical droplet size* related to settling and separation, were compared to deduce this criterion.

Maximum droplet size. Since water is entrained by the flowing oil phase in the form of droplets, it is essential to know the maximum droplet size that can be found in the flow which resists further breakup. Hinze[39] (1955) found that deformation or breakup of droplets occurs if the dynamic pressure force, caused by changes in velocity over a distance approximating the diameter of the droplet, is bigger than the counteracting interfacial tension force. Following Brauner[37] the maximum droplet size, d_{max}, in dilute dispersions can be expressed according to:

$$\left(\frac{d_{max}}{D}\right)_{dilute} = 1.88 \left[\frac{\rho_o(1-\varepsilon_w)}{\rho_m}\right]^{-0.4} We_o^{-0.6} Re_o^{0.08} \tag{15}$$

where:

$$Re_o = \frac{\rho_o D U_c^2}{\eta_o} \qquad We_o = \frac{\rho_o D U_c^2}{\sigma} \qquad f = 0.046/Re_o^{0.2}$$

It should be noted that this equation can only be used in dilute dispersions i.e. as long as it satisfies the following condition:

$$(1-\varepsilon_w)\frac{\rho_o}{\rho_m} \cong 1 \tag{16}$$

In dense dispersions, droplet coalescence takes place. The previous model is not valid for dense dispersion systems and Brauner[37] extended the model to dense dispersion systems. Under such conditions, the flowing oil phase should carry sufficient turbulent energy to disrupt the tendency of the water droplets to coalesce, yielding:

$$\left(\frac{d_{max}}{D}\right)_{dense} = 2.22 C_H^{0.6} \left(\frac{\rho_o U_c^2 D}{\sigma}\right)^{-0.6} \left(\frac{\varepsilon_w}{1-\varepsilon_w}\right)^{0.6} \left[\frac{\rho_m}{\rho_o(1-\varepsilon_w)}f\right]^{-0.4} \tag{17}$$

Thus, given a water-oil fluid system and operational conditions, the maximum droplet size that can be sustained is the larger of the two values obtained via (15) and (17), which can be considered as the worst case for a given oil-water system:

$$\frac{d_{max}}{D} = Max \left\{ \left(\frac{d_{max}}{D}\right)_{dilute}, \left(\frac{d_{max}}{D}\right)_{dense} \right\}$$
(18)

Critical Droplet Size. Droplets larger then a critical droplet size d_{crit} separate out from the two-phase flow dispersion either due to *gravity forces*, predominant in horizontal flow, or due to deformation and "*creaming*" typical for vertical flow.[38] Critical droplet diameter d_{cb} above which separation of droplets due to gravity takes place can be found via a balance of gravity and turbulent forces as:[38]

$$\left(\frac{d_{cb}}{D}\right) = \frac{3}{8} \frac{\rho_o}{|\Delta\rho|} \frac{fU_c^2}{Dg\cos(\theta)} = \frac{3}{8} f \frac{\rho_o}{\Delta\rho} Fr_o$$
(19)

where Froude number is:

$$Fr_o = \frac{U_c^2}{Dg\cos(\theta)}$$

and

$$\Delta\rho = |\rho_o - \rho_w|$$

This effect is predominant at low pipe inclinations i.e. in horizontal and near-horizontal flows. Critical droplet diameter $d_{c\sigma}$ above which drops are deformed and "creamed", leading to migration of the droplets towards the pipe walls in vertical and near-vertical flows, can be calculated with the equation proposed by Brodkley[40]:

$$\left(\frac{d_{c\sigma}}{D}\right) = \left[\frac{0.4\sigma}{|\rho_o - \rho_w| gD^2 \cos(\beta)}\right]^{0.5}$$
(20)

$$\beta = \begin{cases} |\theta| & |\theta| < 45^o \\ 90 - |\theta| & |\theta| > 45^o \end{cases}$$

where θ is the inclination of the pipeline. The critical diameter, d_{crit}, can then be conservatively estimated for any pipe inclination according to the suggestion made by Barnea[38] (1987):

$$\frac{d_{crit}}{D} = Min \left\{ \left(\frac{d_{cb}}{D} \right), \left(\frac{d_{c\sigma}}{D} \right) \right\}$$
(21)

Criterion for Stable Water-in-Oil Dispersion. At this point we are in the position to formulate the final criterion for entrainment. The transition from stratified flow to stable water-in-oil dispersion takes places when the oil phase turbulence is intense enough to maintain the water phase broken up into droplets not larger then d_{max} which has to be smaller than the a critical droplet size d_{crit} causing droplet separation. The transition criterion is then (Brauner[37], 2001):

$$d_{max} \le d_{crit}$$
(22)

Introduction of equations (18) and (21) into (22) leads gives us mean to determine the critical velocity.

Flow Properties Calculation

If the water phase is fully entrained by the flowing oil phase, there is no or very little corrosion risk. However, if the water phase is not entirely entrained and flows separated from the oil phase, it is crucial for corrosion calculations to predict the in-situ water cut, water velocity, water film thickness. This holds for all three main flow regimes considered here. The details of these calculations are given elsewhere[41]. Briefly, the momentum and mass balances are solved for the liquid layer to obtain the superficial velocities of pure water layer, oil-water mixed layer and pure oil layer as well as corresponding layer thicknesses. Once the film thicknesses are calculated, the in-situ velocities of the three layers can be obtained and the information communicated to the corrosion model.

VERIFICATION

Corrosion Model Verification

The corrosion model was verified by comparing the predictions with the large experimental database for CO_2 corrosion and multiphase flow at Ohio University as well as some experimental results from the open literature. A selected number of comparisons is presented below.

The ability of the model to capture fundamental behavior of the CO_2 corrosion process is shown in FIGURE 4. The experimental potentiodynamic sweep was

reproduced by the model successfully showing that under the given set of conditions, direct H^+ reduction is the prevailing cathodic reaction. Using the same series of experiments, FIGURE 5 shows the comparison of corrosion rates as a function of velocity. At pH 5 the corrosion rate has only a mild dependence on flow as the process is controlled by the rate of H_2CO_3 reduction which is under mixed charge-transfer/chemical-reaction control. Similar agreement between the predicted and measured corrosion rates was obtained for pH 4 and pH 6 (not shown here).

The effect of higher CO_2 partial pressure is shown in FIGURE 6. The line labeled the "Electrochemical" model comes from the simplified mechanistic model of George et al.[42] This model includes only the electrochemical reactions as given by equations (1) and (2) and a simplified treatment of mass transfer and chemical reactions as proposed by Nesic et al. [24]. Both models are in good agreement with the experimental data given that in those experiments no protective films formed.

When acetic acid is present in CO_2 corrosion, it can significantly alter the corrosion rate particularly at higher temperature as shown in FIGURE 7. Acetic acid concentration is expressed as total concentration of acetic species (HAc + Ac⁻). In that series of experiments conducted at pH 4 the undissociated form (HAc) prevailed and dominated the corrosion process. One can observe the dramatic increase in the corrosion rate at high acetic acid concentration and the model captures this behaviour well. It should be noted that a similar increase in the corrosion rate is not seen at lower temperatures or at higher pH. At pH 5 the effect of acetic acid is shown in FIGURE 8. At this pH the dominant acetic species is Ac⁻ and the effect on the corrosion rate is not as pronounced since the corrosion rate is dominated by H_2CO_3 reduction due to the higher partial pressure of CO_2 (1.8 bar). Due to its mechanistic nature the model captures this behaviour well.

It can be concluded that the model performs well and predicts successfully the experimentally observed effects of all the influential parameters in CO_2 corrosion, such as: pH, velocity, CO_2 partial pressure, temperature, Fe^{2+} concentration (not shown), HAc, traces of H_2S (not shown), etc. However, other simpler models such as the electrochemical models of George at al.[42], and Anderko et al. as well as the semi-empirical model of de Waard[3] can be just as successful given the chance to calibrate with the same quality experimental data. The difficult test for all these models is corrosion in the presence of iron carbonate films which can be very protective but also partially protective and lead to onset of localized attack. Due to their simplified treatment of transport processes as well as chemical reactions, these models cannot succesfully predict the occurrence of protective films or their protective properties. Therefore the use of correction factors or equivalent adjustable parameters is inevitable. In the present model, the onset of iron carbonate precipitation as well as the growth and protectiveness of iron carbonate films is modelled mechanistically as described by equations (6) and (8). Details about the workings and the capabilities of the film growth model are presented elsewhere[21-23]. When protective iron carbonate films form, the predictions made with the present model and the corrosion rate measurements are compared in FIGURE 9, for the case of "pure" CO_2 corrosion and CO_2/HAc corrosion. The experiments clearly show that protective iron carbonate films formed and reduced the corrosion rate below 0.1 mm/y in all experiments. No effect of acetic acid on the protectiveness of the films was detected in these experiments given that the pH was kept constant. The model predicts the final corrosion rate as well as the absence of acetic acid influence on protectiveness of the iron

carbonate films rather well. SEM analysis (not shown) confirmed the presence of dense iron carbonate films, 10-20 μm thick, as predicted by the model.

Multiphase Flow Model Verification

Flow Pattern Determination

Due to limited access to experimental flow regime data for high pressure multiphase flow in large diameter pipes, a well established code OLGAS 3.0 was used as a benchmark for the current model. A comparison is summarized in the Table 1 below. Flow regime predictions were made for gas-water two-phase flow (100 points) and oil-water-gas three-phase flow (100 points). Range of conditions simulated: pipe diameter 1-50 cm,   pipe inclination: downward vertical and inclined, horizontal, upward inclined and vertical, pressure 1 – 30 bar, superficial liquid velocity 0.1 – 10 m/s, superficial gas velocity 0.1 – 100 m/s.

Table 1. Comparison between the predictions made with present model and a well established commercial flow simulator.

Flow regime	Percentage agreement	
	Gas-water flow	Oil-water-gas flow
Stratified flow	72%	74%
Slug flow	69%	71%
Annular flow	71%	65%

Given the simplicity of the present model in reference to OLGA 3.0 as well as the uncertainty of the OLGA 3.0 predictions, the performance of the present model for flow regime prediction can be considered reasonable for the purposes of corrosion rate calculations.

Water Entrainment/Wetting

A comparison between the experimental results and predictions made by the water entrainment model for different two-phase oil-water flow regimes was done (50 points). The experimental results were obtained from Ohio University's multiphase flow database and open literature (Trallero et al.[43] Angeli and Hewitt[44], and Nadler and Mewes[45]) for pipe diameters 2.5 – 10 cm, atmospheric pressure and a variety of inclinations varying from downward vertical and inclined, horizontal, to upward inclined and vertical flow.

Table 2. Comparison between the predictions made with present model and experimental results from Ohio University's multiphase flow database and open literature (Trallero et al.[43] Angeli and Hewitt[44], and Nadler and Mewes[45]).

Flow regime	Percentage agreement
	Oil-water flow
Stratified flow	80%
Water-in-oil dispersed flow	70%

Given the uncertainty in the experimental results as well as the arbitrariness of some of the constants used in this first version of the water entrainment model the agreement can be considered as reasonable. Other models and rules of thumb (e.g. 1 m/s, 30% water cut) typically used were able to predict with an accuracy just above 50%. when compared with this pool of cases.

Flow Properties Calculation

Comparisons were made between the predicted results by the three-layer model described above and experimental data in oil-water flow (taken form Shi et al.[46]) for input water cuts of 20% and 40%. Typical comparison between the model predictions and experimental results for the pure water layer thickness is shown in FIGURE 10. Given the accuracy of the experimental data, a reasonable agreement between the experimental and the predicted data is achieved, particularly at higher flow rates. More accurate experimental data are needed to calibrate and improve the existing model.

CONCLUSIONS

- The corrosion model was successfully verified with a large experimental database and was able to perform reasonably well in all cases.
- The multiphase flow model was verified against a limited experimental database and benchmarked against a well established commercial package.

FUTURE DEVELOPMENTS

- The predictions made with the present model will be compared with a comprehensive database of field cases.
- A model of corrosion at high H_2S concentrations (% range) will be deveoped which will include the effect of iron sulfide precipitation.
- The effect scale formation (e.g. $CaCO_3$) will be added.

- The effect of more complex water chemistry will be added, including the effect of extreme solution nonideality seen in concentrated brines.
- The effect of glycol/methanol will be added.
- A model of top-of-the-line corrosion, i.e. corrosion under dewing conditions will be added.
- The model of localized corrosion will be further developed and verified against empirical data.

REFERENCES

1. C. de Waard and D. E. Milliams, Corrosion, 31 (1975): p.131.
2 . C. de Waard, U. Lotz, D. E. Milliams, Corrosion, 47 (1991): p. 976.
3. C. de Waard, U. Lotz, A. Dugstad, "Influence of Liquid Flow Velocity on CO_2 Corrosion: A Semi-Empirical Model", CORROSION/95, paper no. 128, (Houston Texas: NACE International, 1995).
4. M. R. Bonis, J.-L. Crolet, "Basics of the Prediction of the Risks of CO_2 Corrosion in Oil and Gas Wells", CORROSION/89, paper no. 466, (Houston Texas: NACE International, 1989).
5. J.-L. Crolet, M. R. Bonis, SPE Production Engineering, 6 (1991): p. 449.
6. Y. M. Gunaltun. "Combining research and field data for corrosion rate prediction". CORROSION/96, paper no. 27. (Houston Texas: NACE International, 1996).
7. A. M. K. Halvorsen, T. Søntvedt, "CO_2 Corrosion Model for Carbon Steel Including a Wall Shear Stress Model for Multiphase Flow and Limits for Production Rate to Avoid Mesa Attack", CORROSION/99, paper no. 42 (Houston, TX: NACE International, 1999).
8. "CO_2 Corrosion Rate Calculation Model", NORSOK standard No. M-506, Norwegian Technology Standards Institution, http://www.nts.no/norsok, June 1998.
9. A. J. McMahon, D. M. E. Paisley, "Corrosion Prediction Modelling - A Guide to the Use of Corrosion Prediction Models for Risk Assessment in Oil and Gas Production and Transportation Facilities", Report No. ESR.96.ER.066, BP International, Sunbury, 1997.
10. C. D. Adams, J. D. Garber, R. K. Singh, "Computer Modelling to Predict Corrosion Rates in Gas Condensate Wells Containing CO_2", CORROSION/96, paper no. 31, (Houston Texas: NACE International, 1996).
11. S. Srinivasan, R. D. Kane, " Prediction of Corrosivity of CO_2 H_2S Production Environments", CORROSION/96, paper no. 11, (Houston Texas: NACE International, 1996).
12. R. C. John et al, "SweetCor: An Information System for the Analysis of Corrosion of Steels by Water and Carbon Dioxide", CORROSION/98, paper no. 20, (Houston Texas: NACE International, 1998).
13. W. P. Jepson, C. Kang, M. Gopal and S. Stitzel, "Model for Sweet Corrosion in Horizontal Multiphase Slug Flow", CORROSION/97, paper no. 11, (Houston Texas: NACE International, 1997).
14. R. Zhang, M. Gopal, W. P. Jepson, "Development of a Mechanistic Model For Predicting Corrosion Rate in Multiphase Oil/Water/Gas Flows", CORROSION/97, paper no. 601, (Houston, TX: NACE International, 1997).

15. B. F. M. Pots, "Mechanistic Models for the Prediction of CO_2 Corrosion Rates under Multi-Phase Flow Conditions", CORROSION/95, paper no. 137, (Houston Texas: NACE International, 1995).

16. A. Anderko, R. Young, "Simulation of CO2/H2S Corrosion Using Thermodynamic and Electrochemical Models", CORROSION/99, paper no. 31, (Houston, TX: NACE International, 1999).

17. E. Dayalan, F. D. de Moraes, J. R. Shadley, S. A. Shirazi, E. F. Ribicki, "CO2 Corrosion Prediction in Pipe Flow Under FeCO3 Scale-Forming Conditions", CORROSION/98, paper no. 51, (Houston, TX: NACE International, 1998).

18. M. Sundaram, V. Raman, M. S. High, D. A. Tree, J. Wagner, "Deterministic Modeling of Corrosion in Downhole Environments", CORROSION/96, paper no. 30, (Houston, TX: NACE International, 1996).

19. M. S. High, J. Wagner, S. Natarajan, "Mechanistic Modelling of Mass Transfer in the Laminar Sublayer in Downhole Systems", CORROSION/2000, paper no. 62, (Houston, TX: NACE International, 2000).

20. R. Nyborg: "Overview of CO_2 Corrosion Models for Wells and Pipelines", CORROSION/2002, paper no. 233 (Houston, TX: NACE International, 2002).

21. M. Nordsveen, S. Nesic, R. Nyborg and A. Stangeland, "A Mechanistic Model for Carbon Dioxide Corrosion of Mild Steel in the Presence of Protective Iron Carbonate Films - Part1: Theory and Verification", Corrosion, Vol. 59, (2003): p. 443.

22. S. Nesic, M. Nordsveen, R. Nyborg and A. Stangeland, "A Mechanistic Model for CO_2 Corrosion of Mild Steel in the Presence of Protective Iron Carbonate Films - Part II: A Numerical Experiment", Corrosion, Vol. 59, (2003): p. 489.

23. S. Nesic, K.-L.J.Lee, "A Mechanistic Model for CO_2 Corrosion of Mild Steel in the Presence of Protective Iron Carbonate Films - Part Ⅲ: Film Growth Model", Corrosion, Vol. 59, (2003): p. 616.

24. S. Nesic, J. Postlethwaite, S. Olsen, Corrosion, "An Electrochemical Model for Prediction of Corrosion of Mild Steel in Aqueous Carbon Dioxide Solutions", 52, (1996): p. 280.

25. S. Nesic, N. Thevenot, J.-L. Crolet, D. Drazic, "Electrochemical Properties of Iron Dissolution in the Presence of CO_2 - Basics Revisited", CORROSION/96, paper no. 3, (Houston, TX: NACE International, 1996).

26. M. L. Johnson and M. B. Tomson, "Ferrous Carbonate Precipitation Kinetics and Its Impact on CO_2 Corrosion", CORROSION/91, paper no. 268, (Houston, TX: NACE International, 1991).

27. E.W.J. van Hunnik, B.F.M. Pots and E.L.J.A. Hendriksen, "The Formation of Protective $FeCO_3$ Corrosion Product Layers in CO_2 Corrosion". CORROSION/96, paper no. 6, (Houston, TX: NACE International, 1996).

28. S. Nesic, W. Wilhelmsen, S. Skjerve and S. M. Hesjevik, "Testing of Inhibitors for CO_2 Corrosion Using the Electrochemical Techniques". Proceedings of the 8th European Symposium on Corrosion Inhibitors, Ann. Univ. Ferrara, N.S., Sez. V, Suppl. N. 10, 1995.

29. C. Mendez, S. Duplat, S. Hernandez, J. Vera, "On The Mechanism Of Corrosion Inhibition By Crude Oils". CORROSION/2001, paper no. 01044, (Houston, TX: NACE International, 2001).

30. S. Hernandez, S. Duplat, J. Vera, E. Baron, "A Statistical Approach For Analyzing The Inhibiting Effect Of Different Types Of Crude Oil In Co2 Corrosion Of Carbon Stee". CORROSION/2001, paper no. 02293, (Houston, TX: NACE International, 2002).

31. S. Hernandez, J. Bruzual, F. Lopez-Linares, J. Luzon, "ISOLATION OF POTENTIAL CORROSION INHIBITING COMPOUNDS IN CRUDE OILS". CORROSION/2003, paper no. 03330, (Houston, TX: NACE International, 2003).

32. S. Nesic, Y. Xiao, B.F.M. Pots "A quasi 2-D localized Corrosion Prediction Model". CORROSION/2004, under review, (Houston, TX: NACE International, 2004).

33. Taitel, Y. and Dukler, A.E., "A Model for Predicting Flow Regime Transitions in Horizontal and Near Horizontal Gas Liquid Flow", AICHE J., Vol.22, No.1, pp.47, 1976

34. Zagarola, M.V., "Mean-flow Scaling of Turbulent Pipe Flow", Ph.D thesis, Princeton University, U.S.A, 1996

35. Petalas, N. and Aziz, K., "A Mechanistic Model for Multiphase Flow in Pipes", Paper No.98-39, the 49th Annual Technical Meeting of the Petroleum Society of the Canadian Institute of Mining, Metallurgy and Petroleum, 1998

36. Jepson, W.P. and R.E., Taylor, "Slug Flow and Its Transitions in Large-Diameter Horizontal Pipes", Int. J. Multiphase Flow, 19, 411-420, 1993.

37. Brauner, N., "The Prediction of Dispersed Flows Boundaries in Liquid-Liquid and Gas-liquid Systems", Int. J. of Multiphase Flow, Vol.27, pp. 885~910(2001)

38. Barnea, D., "A Unified Model for Predicting Flow Pattern Transitions for the Whole Range of Pipe Inclinations", Int. J. of Multiphase Flow, Vol.11, pp. 1~12(1987)

39. Hinze, J., "Fundamentals of the Hydrodynamic Mechanism of Splitting in Dispersion Process", AICHE, Vol. 1(1955), No. 3, pp. 289~295

40. Brodkey, R.S., " The Phenomena of Fluid Motions", Addison-Wesley, Reading, M.A., 1969

41. J. Cai, S. Nesic, C. De Waard, " Modeling of Water Wetting in Oil-Water Pipe Flows". CORROSION/2004, under review, (Houston, TX: NACE International, 2004).

42. K. George and S. Nesic, "Electrochemical Investigation of CO_2 Corrosion of Mild Steel in the Presence of Acetic Acid – Experimental Results, Electrochemical Modeling and a Modification to the de Waard Corrosion Model". CORROSION/2004, under review, (Houston, TX: NACE International, 2004).

43. Trallero, J. L, Sarica, C and J. P. Brill, "A Study of Oil-Water Flow Patterns in Horizontal Pipes", SPE, Paper No. 36609, 363-375, 1996

44. Angeli, P., and Hewitt, G. F, "Drop Size Distributions in Horizontal Oil-Water Dispersed Flows", Chem. Eng. Sci. 55, 3133-3143, 2000

45 Nadler, M. and Mewes, D, "Flow Induced Emulsification in the Flow of Two Immiscible Liquids in Horizontal Pipes", Int. J. Multiphase Flow, 23, 56-68, 1997

46. Hua Shi, Hongbin Wang and W.P. Jepson, "Prediction of water Film Thickness and Velocity for Corrosion Rate Calculation in Oil-Water Flows", NACE 2002, Paper No.02500, pp. 1-18, 2002

47. S. Nesic, G. T. Solvi, and J. Enerhaug, Corrosion, "Comparison of the Rotating Cylinder and Pipe Flow Tests for Flow-Sensitive Carbon Dioxide Corrosion", 51, (1995): p. 773.

48. S. Nesic, and S. Wang, " High Pressure CO_2 Corrosion Electrochemistry". CORROSION/2004, under review, (Houston, TX: NACE International, 2004).

49. A. Smeltz, " Electrochemical Investigation of CO_2 Corrosion of Mild Steel in the presence of Acetic Acid". Sep. 2003, Board Meeting report, Ohio University.
50. K. Chokshi, " A study of Inhibitor – Scale Interaction in CO_2 Corrosion of Mild Steel". Sep. 2003, Board Meeting report, Ohio University.
51. W. Sun, " Kinetics of Scale formation in CO_2/H_2S Solution". Sep. 2003, Board Meeting report, Ohio University.
52. O. Nafday, " Film Formation and CO_2 Corrosion in the presence of Acetic Acid". Sep. 2003, Board Meeting report, Ohio University.

ACKNOWLEDGMENTS
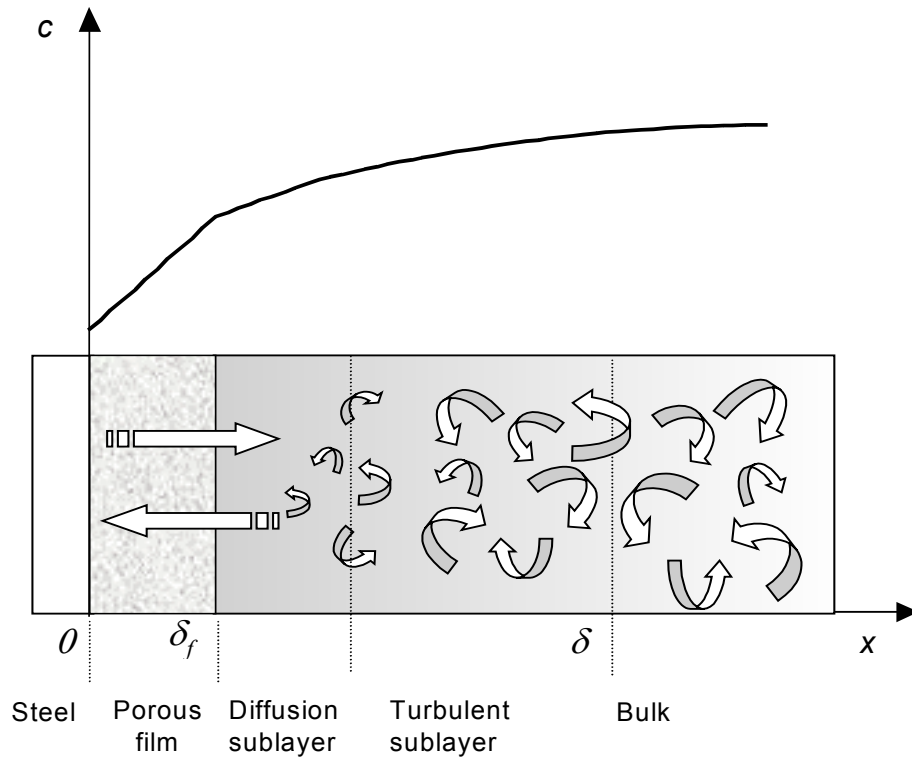
FIGURE 1. Sketch of the computational domain and a typical concentration profile for a dissolved species.
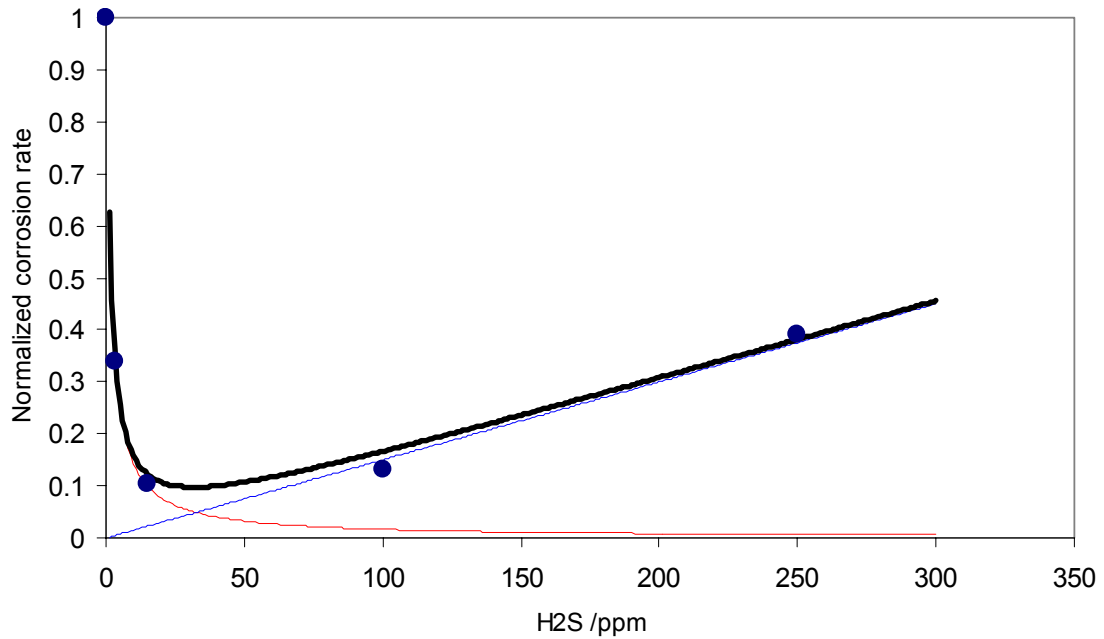
FIGURE 2. Effect of low concentrations of H_2S on the CO_2 corrosion rate in the absence of iron sulphide precipitation. ppm refers to the concentration in the gas phase.
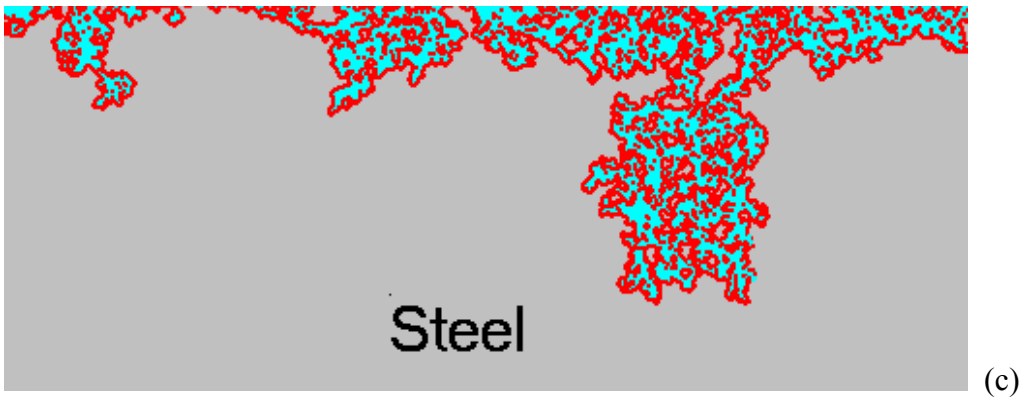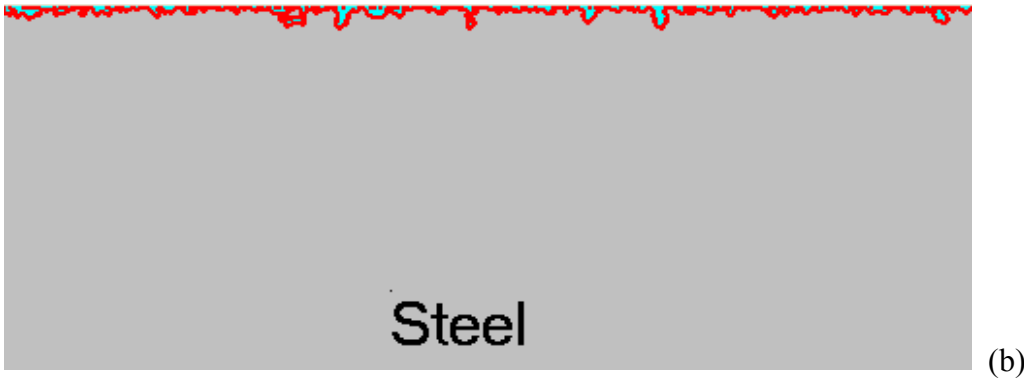
FIGURE 3. Samples of simulated metal surface morphology for the cases of (a) zero scaling tendency (b) high scaling tendency and (c) moderate scaling tendency.
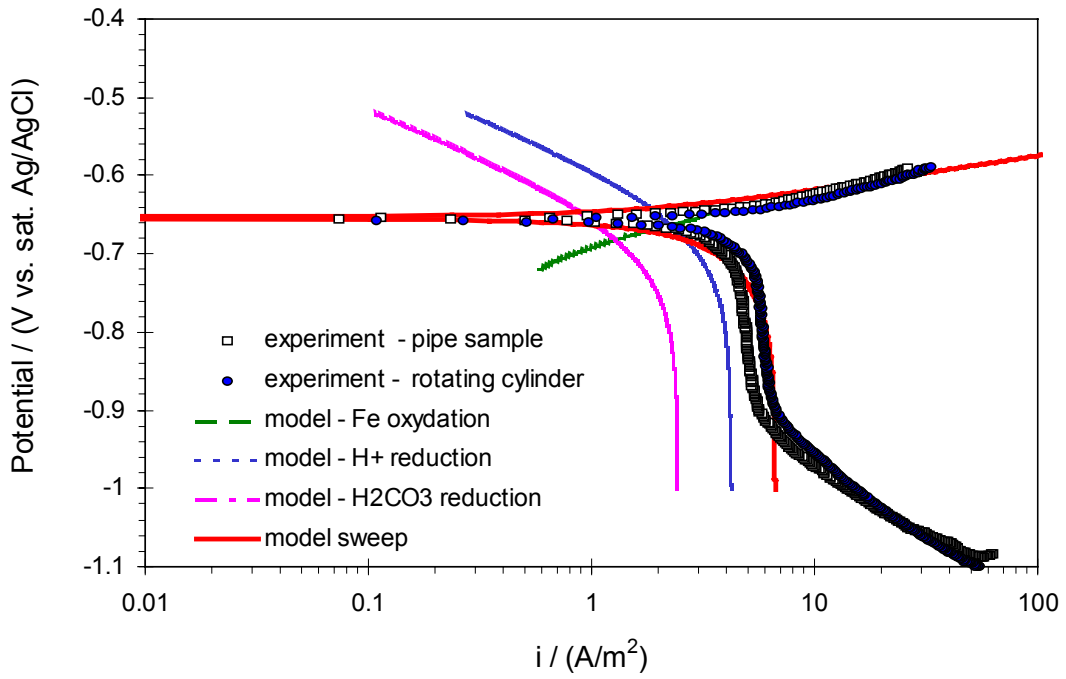
FIGURE 4. Comparison of predicted and measured potetiodynamic sweeps. Test conditions: pH 4, 20°C, 1 bar CO_2, 2 m/s. Data taken from Nesic et al[21].
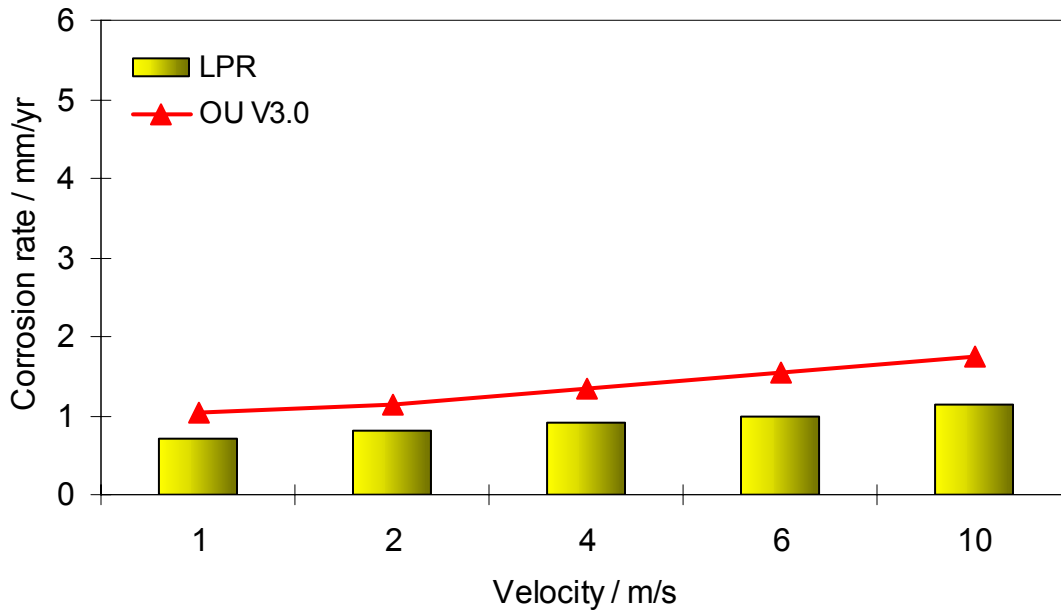
FIGURE 5. Comparison of the predicted and experimentally observed corrosion rates as a function of velocity. Test conditions: pH 5, 20°C, 1 bar CO_2. Data taken from Nesic et al[47].
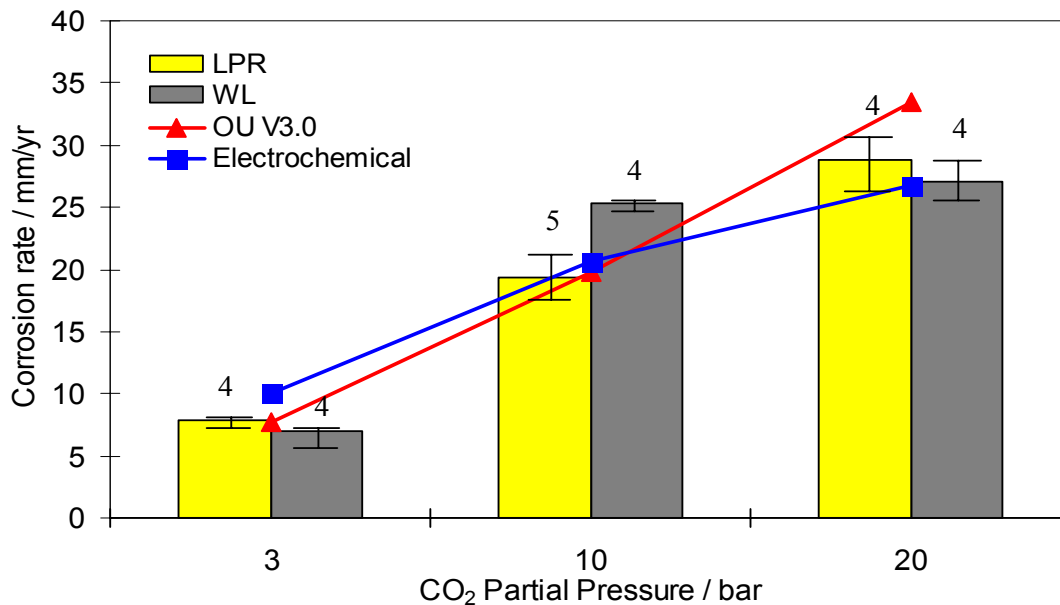
FIGURE 6. Comparison of predictions and experimentally measured corrosion rates showing the effect of CO_2 partial pressure. Test conditions: 60^oC, pH 5, 1 m/s. Data taken from Wang et al[48]. Corrosion rates were measured both by linear polarization resistance (LPR) and weight loss (WL). Error bars denote max/min values and the figure above the bars is the number of repeated experiments.
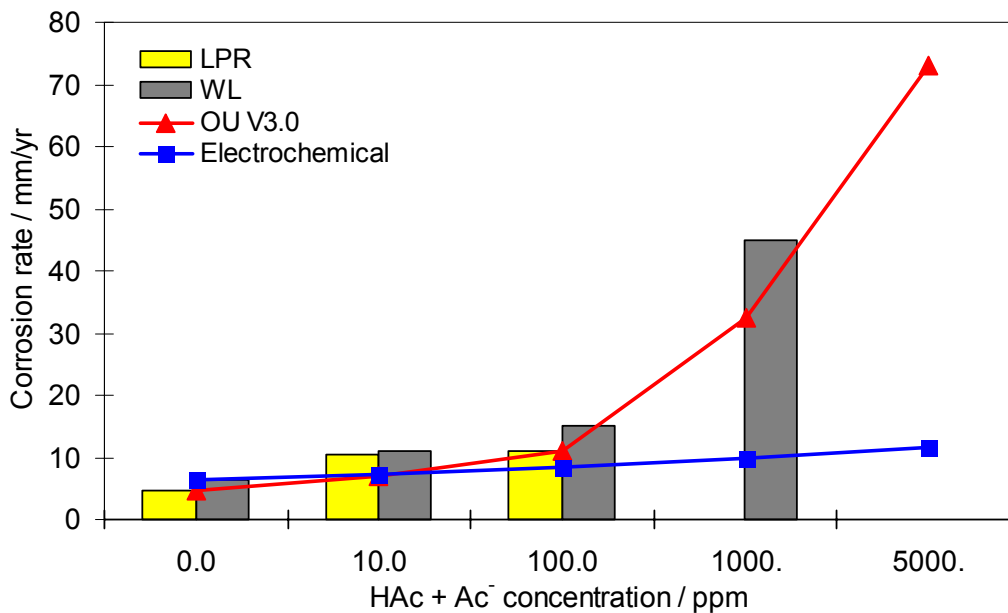

FIGURE 7. Comparison of predictions and experimentally measured corrosion rates showing the effect of acetic acid on CO_2 corrosion. Test conditions: 60^oC, $pCO_2 = 1.0$ bar, pH 4, 0.5 m/s. Data taken from George et al[42]. Corrosion rates were measured both by linear polarization resistance (LPR) and weight loss (WL).
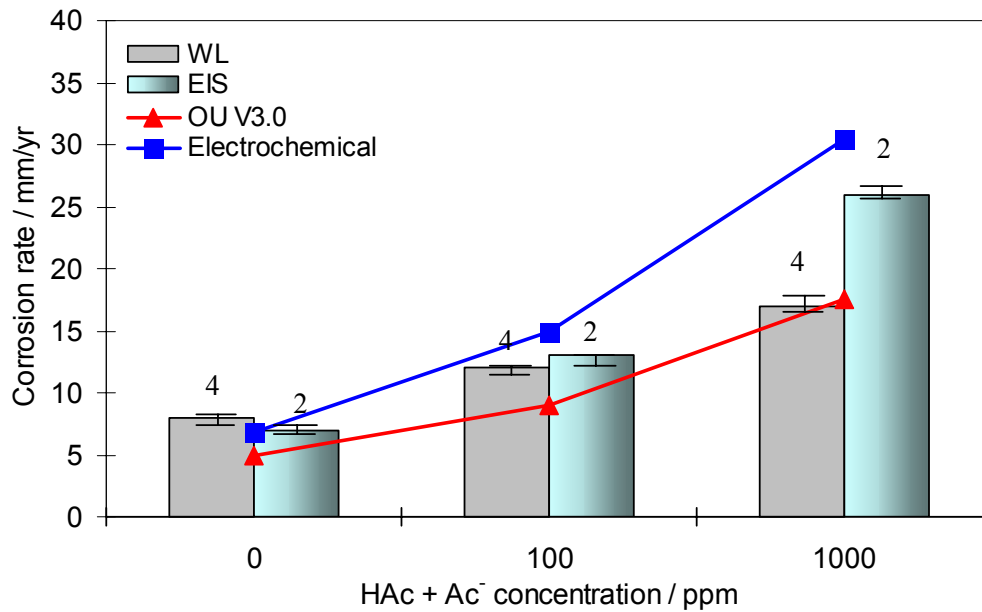
FIGURE 8. Comparison of predictions and experimentally measured corrosion rates showing the effect of acetic acid on CO_2 corrosion. Test conditions: $60^{\circ}C$, $pCO_2 =1.8$ bar, pH 5, 1 m/s. Data taken from Smeltz[49]. Corrosion rates measured both by Electrochemical Impedance Spectroscopy (EIS) and weight loss (WL). Error bars denote max/min values and the figure above the bars is the number of repeated experiments.
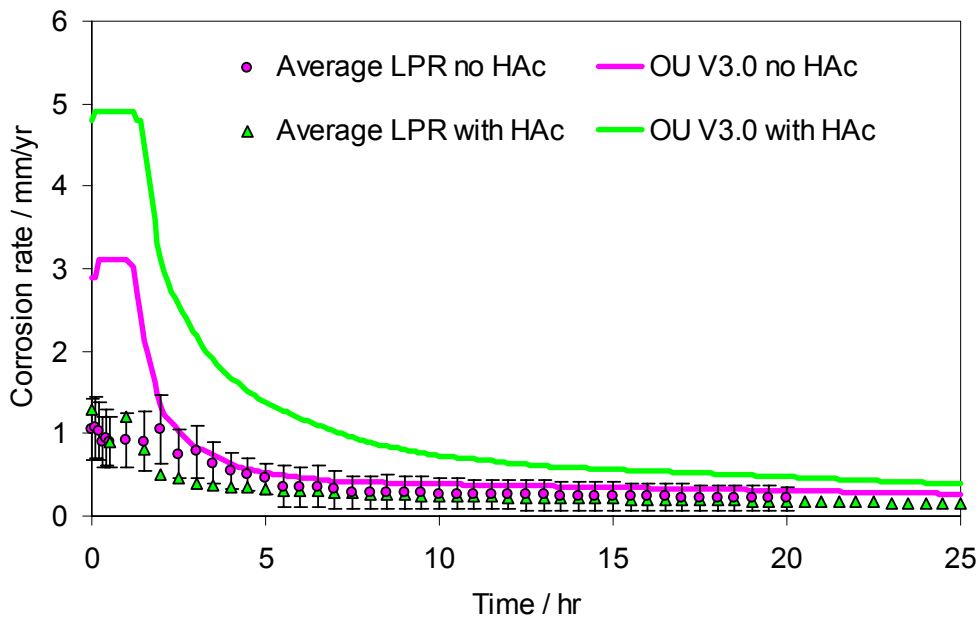

FIGURE 9. Comparison of predictions and experimentally measured corrosion rates showing the effect of protective iron carbonate films for the case of CO_2 corrosion with and without acetic acid. Test conditions: $80^{\circ}C$, $pCO_2 =0.54$ bar, pH 6.6, stagnant, 1000 ppm acetic acid (HAc +Ac⁻). Data taken from Chokshi[50], Sun[51] and Nafday[52]. Error bars denote one standard deviation.
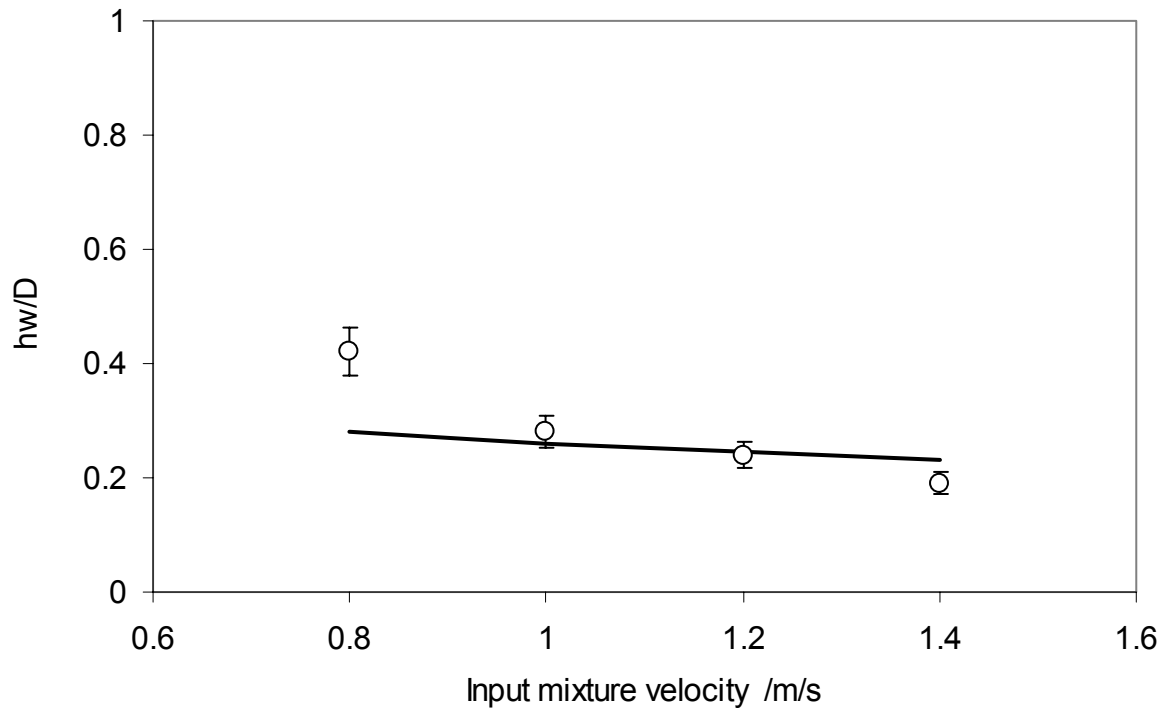
FIGURE 10. Comparison between the predicted pure water layer thickness and experimental data of Shi et al.[46] at nominal water cut of 40%.